Received: 23 November 2021 | Revised: 3 January 2022 | Accepted: 31 January 2022

IET Electrical Systems in Transportation

DOI: 10.1049/els2.12043

The Institution of Engineering and Technology WILEY

ORIGINAL RESEARCH

Study on electric spark discharge between pantograph and catenary in electrified railway

Hongyi Zhou[1] | **Fuchuan Duan**[2] | **Zhigang Liu**[1] | **Long Chen**[1] | **Yang Song**[3] | **Yexin Zhang**[1]

[1]College of Electrical Engineering, Southwest Jiaotong University, Chengdu, China

[2]College of Transportation Engineering, Tongji University, Shanghai, China

[3]Department of Structural Engineering, Norwegian University of Science and Technology, Trondheim, Norway

Correspondence

Fuchuan Duan, College of Transportation Engineering, Tongji University, Shanghai 201804, China.
Email: duanfc_cd@outlook.com

Funding information

National Nature Science Foundation of China, Grant/Award Number: U1734202; Science and Technology Innovation Talents of Sichuan Science and Technology Plan, Grant/Award Number: 2021JDRC0008; Research Project of China Railway Eryuan Engineering Group Co. Ltd., Grant/Award Number: KYY2020033(20-21)

Abstract

The electric spark caused by pantograph-catenary (PC) electrical contact failure happens frequently, it is a kind of arcing phenomenon which can severely affect the current collection of PC. The theoretical analysis and modelling of PC electric spark are tried. First, the contact spots between PC and their temperature rise are analysed and derived based on the classical electrical contact theory, respectively. The mechanism of spark discharge is revealed through the analysis of PC voltage difference, and the spark discharge model is proposed combining with the spot temperature rise formula and spark discharge mechanism. Then, in order to obtain some key parameters in an electric spark discharge model, such as contact force and contact current, the structure model of PC and the circuit model of vehicle-grid are established for the calculation of the spark rate in PC. Finally, the spark rate is calculated and analysed under the different parameters in PC system. The calculation results are verified by the experiment results. Through the presentation of the correlation of electric spark discharge and factors, such as contact force, contact current and material of PC, this study can support the assessment of electrical contact quality in the PC system in future study.

KEYWORDS

electric spark discharge, electrified railway, pantograph-catenary electrical contact, traction power

1 | INROTDUCTION

In recent years, the high-speed and heavy load are the main trends of electrified railways in China. With the increase of train speeds, the interaction of pantograph-catenary (PC), which is influenced by irregularities of catenary and tracks [1], catenary defects [2], vibration of pantograph and other factors, becomes more intense and complex [3]. The electrical contact state of PC is unstable and the electric spark phenomenon (as shown in Figure 1) regularly occurs.

The electric spark between PC is a violent discharge phenomenon due to the high voltage of PC system, it is a kind of arcing phenomenon which will cause burning of contact wire, over voltage on pantograph and electromagnetic interference problems of PC system, and it seriously affects the current collection of PC. Therefore, it is essential to study the mechanism and influence of PC electric spark.

In order to ensure the security of PC current collection, many research studies have been carried out in PC system, including PC interaction dynamics, PC electrical contact and PC arc detection. The research studies of PC interaction dynamics include the system algorithm of PC [4, 5] and control strategy of contact force [6, 7], which can provide assessment of PC current collection quality. For the research studies of PC electrical contact, Holm analysed the microscopic structure of contact face and put forward the concept of contact resistance

FIGURE 1 Electric spark on pantograph-catenary

[8]; on this basis, many research studies refined the mathematical form of contact resistance [9, 10] and revised the contact resistance model considering external factors of contact face [11–13]; combined with the electric contact theory many experiments of PC electrical contact have been carried out [14–16] and reflected the influence of practical PC factors on current collection quality. The research studies of PC arc detection include the methods of data detection [17, 18] and image detection [19, 20], which can provide forecast for PC contact failure.

The above research studies provide indirect support for ensuring PC current collection; however, there are few research studies on the PC spark phenomenon which directly reflects the quality of PC current collection. For the spark discharge, research studies have been carried out include its conditioning [21], modelling [22] and characteristics analysis [23]; therefore, they are not suitable for studying the PC spark discharge which occurs under the PC slide contact with high voltage, high speed and fluctuant contact force [24].

Aiming at the electric spark phenomenon in the PC electrical contact process, the mechanism of electric spark is discussed in detail, and the model for electric spark discharge is built considering practical factors in the PC system. Then, the spark rate under different conditions of PC system is calculated and analysed, which can provide an assessment for electrical contact state of PC system. The main contents of this paper are shown in Figure 2.

2 | MODELLING OF ELECTRIC SPARK

In order to reveal the mechanism of electric spark discharge in the PC system, it is very essential to analyse the contact spots between PC, which are the microstate of PC electrical contact as well as the temperature rise of contact spots, which is the cause of spark. During the analysis process, the relevant formulae are mathematically derived considering practical factors in the PC system and form the electric spark discharge model, as described in the following sections.

In electrified railways, trains obtain current through the contact of PC, as shown in Figure 3a. In the operation of trains, under the uplift force of pantograph, the pantograph tightly withstands catenary and the current passes through two contact surfaces, which forms a process of sliding electrical contact, as shown in Figure 3b. Due to the irregularity of the contact material in microcosmic, the contact of PC is realised by the microcosmic contact spot, as shown in Figure 3c and Figure 3d.

2.1 | Contact spot and its temperature rise in pantograph-catenary system

In the theory of electrical contact, the contact surface of two solids is rugged on the microstructure, and the contact of two components is represented as discontinuous spots, which are formed by an external force acting on the rugged contact surface [25]. It is obvious that the electrical contact system of PC has the same microstate, as shown in Figure 3c and Figure 3d.

According to the electrical contact theory in Ref. [10], the actual passageways for current are the small conductive spots named '*a*-spot', when the current passes through two components. The current lines contract when the current passes through *a*-spot (as shown in Figure 4a), which leads to the increase of resistance, and the increment of resistance is called the constriction resistance. The oxide film of the contact surface will affect the formation of constriction resistance and generate another increment of resistance called the membrane resistance. The above two resistances form the contact resistance.

Considering the operation environment of high current in the PC system, the oxide film will be destroyed in such environments [24]; therefore, the membrane resistance can be ignored and the contact resistance is equal to the constriction resistance.

The *a*-spot has a variety of shapes, which will influence the contraction of the current and affect the value of contact resistance. According to the experimental measurement [24] of contact spots with the same area but different shapes, it is found that the contact resistance calculated by circular contact spots is in the middle value, which are considered to be suitable for engineering calculation. The circular *a*-spot is taken as the basic assumption.

Assume the radius of *a*-spot is a/m; in the process of the current contracting to *a*-spot, the equipotential surfaces of two components near *a*-spot are a series of ellipsoids [10] (as shown in Figure 4b); through integrating the equipotential surface the contact resistance of a single *a*-spot can be calculated as

$$R = \frac{\rho}{2a} \tag{1}$$

Considering pantograph-catenary system, the contact resistance is

$$R = \frac{\rho_1 + \rho_2}{4a} \tag{2}$$

where ρ_1 and ρ_2 are the resistivity of pantograph and catenary, respectively.

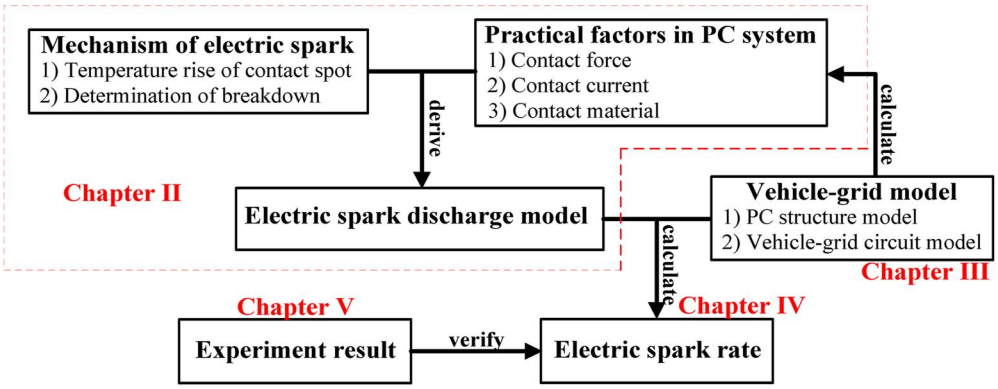

FIGURE 2 Main contents of this paper

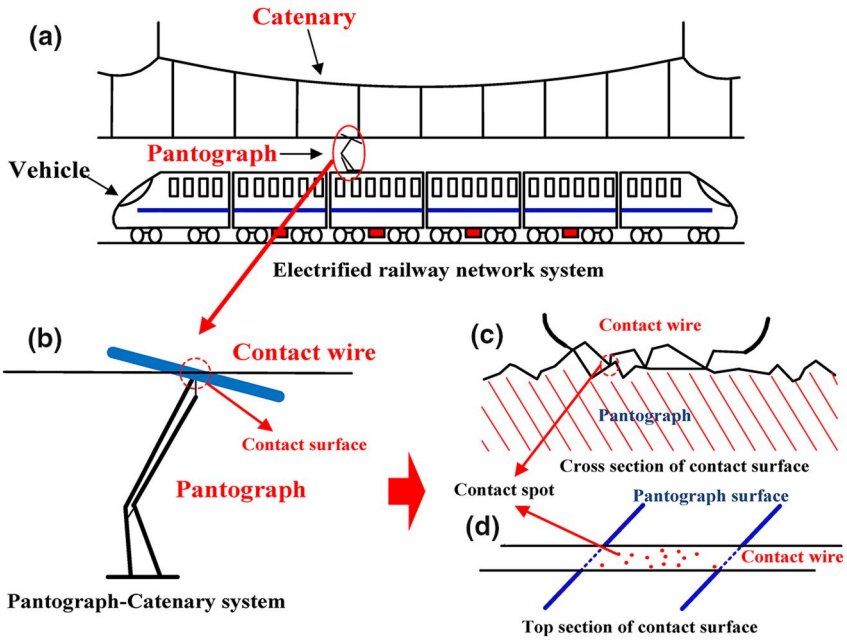

FIGURE 3 Electrified railway network system and pantograph-catenary system

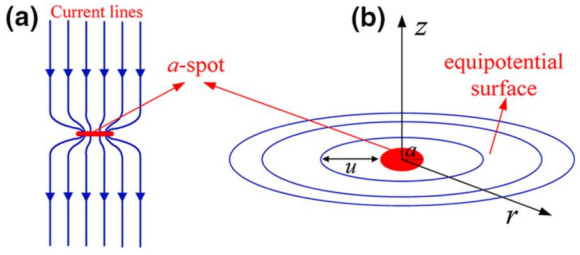

FIGURE 4 A-spot and its equipotential surfaces

In the microstructure of PC contact surface, due to the irregularity of the material surface, the contact surface is actually formed by the contact of irregular hillocks (as shown in Figure 5a). Under the assumption of circular contact spot, the shape of hillocks can be regarded as hemispherical [26], and they are pressed to form circular contact spots under the action of PC contact force F_n (as shown in Figure 5b and Figure 5c).

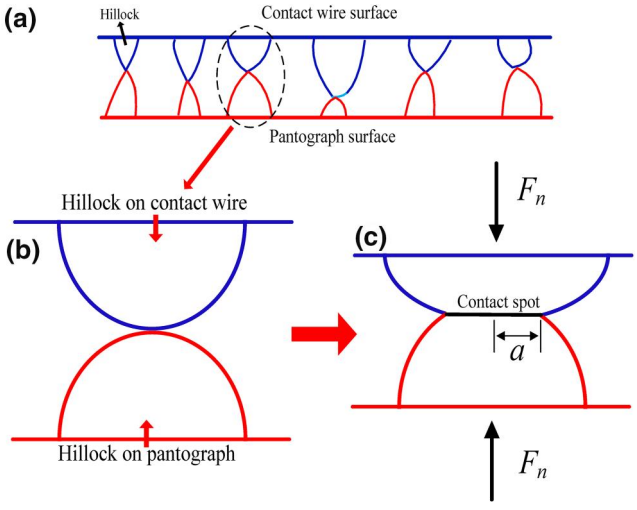

FIGURE 5 Microstructure of pantograph-catenary contact surface

Based on the circular *a*-spot model, assume that the number of *a*-spot in the PC contact surface is n, and each spot has the same radius a/m. Considering the order of magnitude of the distance between each spot in the PC electrical contact system is much larger than the size of spot itself [24], each contact resistance of *a*-spot can be equivalent to be parallel (as shown in Figure 6). When the voltage drop of *a*-spot is V, the temperature rise of *a*-spot can be expressed by Kohlraush's equation [27].

$$V^2 = 8\int_{\theta_0}^{\theta_m} z(\theta)g(\theta)d\theta \tag{3}$$

where θ_m and θ_0 are the absolute temperature of *a*-spot and remote regions of conductor, $z(\theta)$ is the distribution of material thermal conductivity with temperature, and $g(\theta)$ is the distribution of material electrical resistivity with temperature.

If an approximate calculation is considered [24], the Wiedemann-Franz law (the product of electrical resistivity and thermal conductivity is proportional to the temperature rise $z(\theta)g(\theta) = L\theta$, where the scale factor L is Franz constant) can be used to simplify the integral of temperature in (3). The Wiedemann-Franz law applies to the materials such as copper, silver and gold and their alloy, which is suitable for the material of contact wire in the PC system.

Based on the equivalent model of PC contact in Figure 6, assume the current passing through two conductors is I, and combining with (2), the voltage drop on a single spot can be expressed as

$$V = R_n\frac{I}{n} = \frac{(\rho_1+\rho_2)I}{4na} \tag{4}$$

Considering the microscopic parameter a (radius of *a*-spot) cannot be used for engineering calculation [26], in the contact system with current, the current density of contact spot can be used to convert parameter a at the macro level. Based on the *a*-spot model, the current density of each round spot is

$$J = \frac{I}{n\pi a^2} \tag{5}$$

where J is the current density on the contact spot.

Combining (3), (4) and (5), the temperature of contact spot can be expressed as

$$\theta_m = \sqrt{\frac{J(\rho_1+\rho_2)^2\pi I}{64Ln} + \theta_0^2} \tag{6}$$

It can be found from (6) that the temperature rise of contact spot is mainly influenced by the current density and the number of *a*-spot under the condition of constant current value, but the current density J on contact spot is difficult to obtain in the PC system, and considering the feasibility of engineering calculation, the contact force acting on contact spot is used to convert the current density [26], which can be detected and simulated in the PC system.

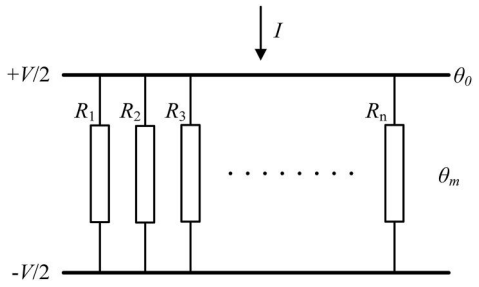

FIGURE 6 Equivalent model of a-spot between pantograph-catenary

Considering that the contact surface is formed by force extrusion of hemispherical hillock of two contact materials (as shown in Figure 5c), the contact surface conforms to *a*-spot model. According to the definition of material hardness, for the soft one of two contact conductors, it can be found that

$$H = \frac{F_n}{S} = \frac{F}{n\pi a^2} \tag{7}$$

where F_n and S are the contact force and area of single *a*-spot, F is the contact force of PC, and H is the hardness of the soft one of two contact conductors.

Combining (5) and (7), and considering the decreasing of hardness caused by high currents [24], the current density can be expressed as

$$J = \frac{\mu IH}{F} \tag{8}$$

where μ is a constant that indicated the hardness reduction.

Combining (6) and (8), it can be found that

$$\theta_m = \sqrt{\frac{\pi\mu HI^2(\rho_1+\rho_2)^2}{64nLF} + \theta_0^2} \tag{9}$$

Based on the above derivation, a temperature rise algorithm (9) of contact spot, which can be used in engineering calculation is obtained. It can be found that the temperature rise of contact spot in the PC system is mainly influenced by contact current I, contact force F, number of contact spot n and the contact material (hardness H of contact wire and resistivity ρ_1 and ρ_2 of pantograph and catenary).

2.2 | Mechanism of electric spark discharge in the pantograph-catenary system

According to (9) derived in the previous section, the effects of current and contact force will heat the contact spot. The absolute temperature θ_m of contact spot will reach the boiling point of the contact material under certain current value and contact force value. When the contact spot vaporises, the electrical contact of two hillocks will be interrupted. In the above situation, breakdown will occur if voltage difference

exists between electric contact; it will cause the arcing phenomenon and combustion, which present as spark discharge.

The experiment of graphite-copper contact in Ref. [27] shows the spark discharge will occur under sufficient voltage difference after contact spot vaporisation, and the voltage is 10–20 V by measurement.

In the traction system of electrified railway, the traction substation transmits electric energy to train through the PC system by a 27.5 kV sinusoidal alternating current voltage. If the contact spots between PC vaporise, the PC will be in a temporary detachment state until the contact spots regenerate under the action of relative motion of the PC, as shown in Figure 7a. Assume the contact spots vaporise at time t_0, and the detachment duration is Δt; the voltage between PC is shown in Figure 7b. At the spots vaporise time t_0, the voltages of pantograph slipper and contact wire are at point A in Figure 7b. Considering the detachment duration Δt is extremely short, the voltage of pantograph slipper will be still at point A during Δt because of detachment, and the voltage of contact wire will change to point B because of continuous power supply by traction substation.

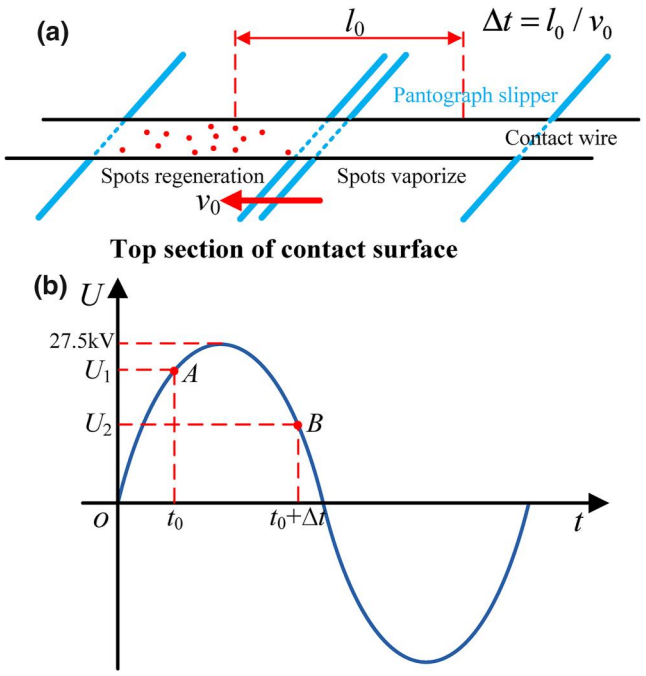

FIGURE 7 Detachment process and voltage of pantograph-catenary

In the process from point A to point B in Figure 7b, a continuously changing voltage difference ΔU_t will exist between PC. The maximum value of absolute value of ΔU_t can be expressed as

$$\Delta U_m = U_m \cdot \max|\sin(\omega t_0) - \sin[\omega(t_0 + \Delta t_x)]| \qquad (10)$$

where U_m = 27.5 kV, $\Delta t_x \in [0, \Delta t]$, $\omega = 100\pi$.

If the value of ΔU_m can reach the test result of the experiment in Ref. [27], the electric spark discharge between PC will occur when the contact spots vaporise. Considering the monotonicity of (10), ΔU_m can reach the minimum value when the value of Δt is minimum. According to the spots regeneration process in Figure 7a, the minimum value of l_0 is the width of the actual contact surface of PC (25 mm in average), and below the train speed v_0 = 300 km/h, the minimum value of Δt is about 3×10^{-4}s. Under the above parameters, the values of ΔU_m corresponding to all the points of t_0 within a cycle of sinusoidal voltage in Figure 7b are calculated by MATLAB software which is shown in Figure 8; the time steps of t_0 and Δt are 2×10^{-6}s and 3×10^{-8}s, respectively.

It can be found in Figure 8 that the minimum value of the calculation results of ΔU_m is about 21.3 V, which satisfies the test result of experiment in Ref. [27]. The calculation results show that the minimum value of ΔU_m meets the voltage of spark discharge, and it can be inferred that the spark discharge occurs if the contact spots vaporise below the train speed of 300 km/h in the PC system.

Based on the above analysis, the mechanism of electric spark discharge between PC can be obtained; the process is shown in Figure 9.

The mechanism of spark discharge in Figure 9 reveals that the temperature rise of the contact spot is the main factor of electric spark occurrence, and the (9), which describes that the

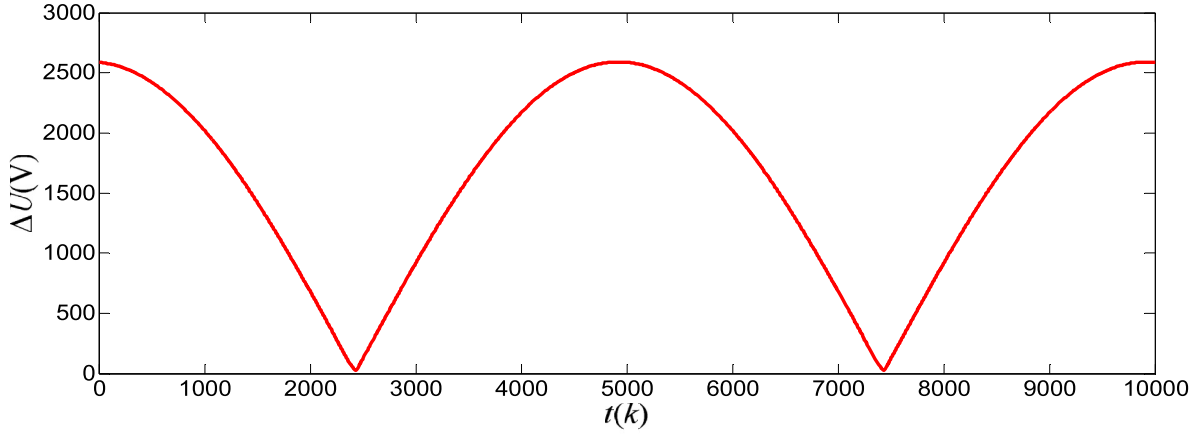

FIGURE 8 Calculation results of ΔU_m

temperature rise of the contact spot can serve as the electric spark discharge model. The electric spark model can determine the occurrence of spark discharge of PC and calculate the spark rate under certain parameters of contact current, contact force and material coefficients in the PC system.

3 | MODELLING FOR PARAMETERS CALCULATION

The spark rate, which can reflect the frequency of spark occurrence, is an important factor to evaluate the electrical contact quality of PC, and in order to calculate the accurate spark rate through the electric spark discharge model, the relatively accurate parameters in (9) need to be obtained, especially contact force and contact current. Therefore, the dynamic model of pantograph and catenary is established to obtain the contact force, and the circuit model of vehicle-grid is established to obtain the contact current.

3.1 | Dynamic structure model of pantograph-catenary

For the pantograph, a lumped-parameter model is established to analyse its dynamic behaviours, as shown in Figure 10.

The pantograph is a three-level model; m_i ($i = 1,2,3$) is the mass of pantograph head, upper frame and lower frame, respectively; k_i ($i = 1,2,3$) represents the stiffness of each parts, c_i ($i = 1,2,3$) denotes the damping, and x_i ($i = 1,2,3$) is the displacement of each part. The motion equation can be expressed as

$$M\ddot{x} + C\dot{x} + Kx = F \tag{11}$$

where M, C and K are the mass, damping and stiffness matrices of pantograph, respectively. The matrix F represents external force vectors and contains the contact F_{pc} and static lift force F_0, as shown in Figure 10.

For the catenary, a non-linear finite element procedure [28] is utilised to model its non-linear behaviours. As shown in Figure 11, a simple suspension catenary is mainly constructed by message wire, droppers and contact wire.

The contact wire and messenger wire are modelled by the non-linear cable element, which can properly reflect their geometrical non-linearities. The droppers are modelled by non-linear truss element that can only withstand tension and cannot be compressed. The equation of motion for the catenary system can be expressed by

$$M_1\ddot{y} + C_1\dot{y} + K_1 y = F_1 \tag{12}$$

where M_1, C_1 and K_1 are the mass, damping and stiffness matrices of catenary, respectively, and y is the global displacement vector.

The interaction between the pantograph and catenary is realised by means of the penalty function method. A number of validations for the PC model have been conducted in the previous studies [29–31]. Here, the verification is presented in Table 1, which shows the comparison between the simulation results and EN 50,318.

3.2 | Vehicle-grid model

The model of vehicle-grid is built by Simulink, which mainly considers the vehicle, traction network and AT traction substation in the vehicle-grid system (as shown in Figure 12).

The model of traction network (as shown in Figure 12) is established by multiconductor theory, and every electrified line in a traction network such as contact wire, messenger wire and rail is considered to be associated with other lines in which the coupling of inductance between lines is considered. The value

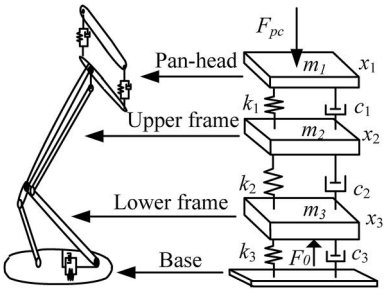

FIGURE 10 Three-level model of pantograph

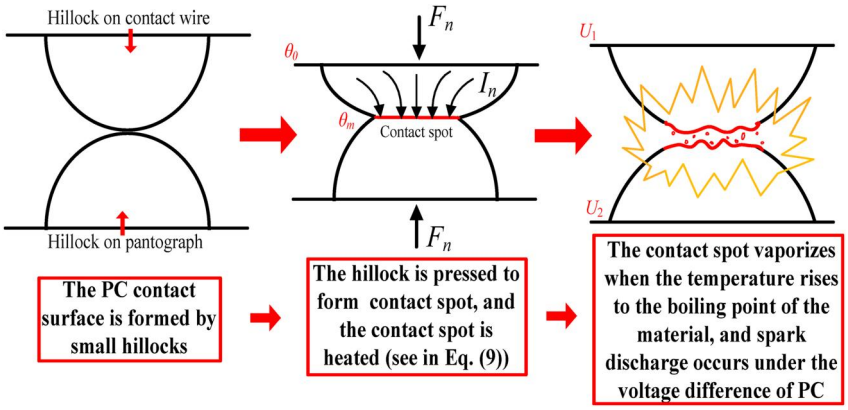

FIGURE 9 Mechanism of electric spark discharge

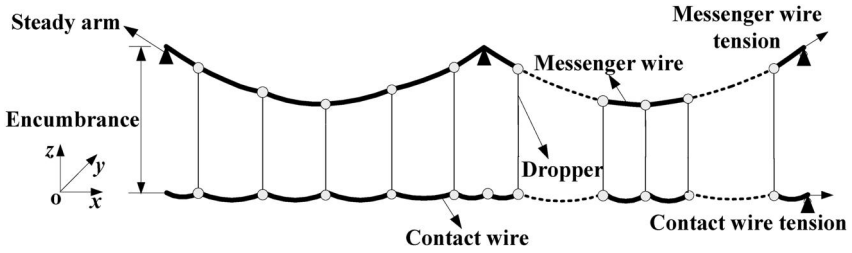

FIGURE 11 Suspension model of catenary

TABLE 1 Validation of the pantograph-catenary model according to EN 50,318

Statistical index	Ranges of the standard results		Computation results	
Speed [km/h]	250	300	250	300
Mean contact force (N)	110~120	110~120	118.30	118.06
Standard deviation (N)	26~31	32~40	26.72	34.87
Max. statistic value (N)	190~210	210~230	198.46	222.67
Min. statistic value (N)t	20~40	−5~20	38.14	13.45
Max. real value (N)	175~210	190~225	191.13	208.04
Min. real value (N)	50~75	30~55	65.79	46.76
Max. uplift at support(mm)	48~55	55~65	52.06	60.73
Percentage of the loss of contact	0%	0%	0%	0%

per unit length of coupling of inductance on each conductor can be calculated by

$$l=\frac{\mu}{2\pi}\left(\ln\frac{\sqrt[n\times m]{\left(\prod_{i=1,j=1}^{n,m}s_{i,j}{}^{(n+m)k_p}\right)^n}}{\sqrt[m]{\left(\prod_{j=1}^{m}r_{0j}{}^{k_j'}\prod_{j=1,p>j}^{m-1,m}d_{0jp}{}^{k_j'+k_j''}\right)}}+\ln\frac{\sqrt[n]{\prod_{i=1,j=1}^{n,m}s_{ij}{}^{k_p'}}\sqrt[m]{\prod_{i=1,j=1}^{n,m}s_{ij}{}^{k_p''}}}{\sqrt[n]{\left(\prod_{i=1}^{n}r_{1j}{}^{k_i'}\prod_{i=0,q>i}^{n-1,n}d_{1jq}{}^{k_i'+k_i''}\right)}}\right) \tag{13}$$

where μ is the vacuum permeability, m and n are the number of transmission and return conductors, s is the distance between two conductors, r is the radius of the conductor itself, and k is the current distribution coefficient of every circuit.

The vehicle is modelled based on CRH380BL-type Electric Multiple unit (see vehicle in Figure 12 which refers to Ref. [32]). The vehicle and the grounding device are equivalent to resistance.

The converter modules including rectifier, inverter and traction motor are connected to the secondary side of the on-board transformer. Especially, the transient direct current control strategy is used in the rectifier, and according to the field oriented vector control method, the feedforward voltages of d axis and q axis of the asynchronous motor are calculated by

$$\begin{cases} U_{sd}^{*}=R_s i_{sd}^{*}-\omega_s L_s\sigma i_{sq}^{*} \\ U_{sq}^{*}=R_s i_{sq}^{*}+\omega_s L_s i_{sd}^{*} \end{cases} \tag{14}$$

where $i_{sd}{}^{*}$and $i_{sq}{}^{*}$ are the stator current of d axis and q axis, respectively, R_s is the resistance of each phase winding of stator, L_s is the self-inductance of equivalent two phase winding of stator, and ω_s is the magnetic field speed of rotor. The parameter ω_s is directly related to vehicle speed, and through changing it, the PC currents under different vehicle speeds can be obtained by simulations. The specific simulation parameters of vehicle [32, 33] are shown in Table 2.

4 | CALCULATION AND ANALYSIS OF ELECTRIC SPARK RATE

According to the modelling and analysis, the occurrence of electric spark can be calculated. The specific calculation process is shown in Figure 13.

In Figure 13, the static parameters P_s include L, μ and θ_0 in (9). The constant is $L = 2.54 \times 10^{-8}\mathrm{V}^2\mathrm{deg}^{-2}$ according to the Wiedemann-Franz law. Based on the data from friction experiments in Ref. [24], the hardness reduction constant is $\mu = 0.85$, and the normal atmospheric temperature is $\theta_0 = 293.15$ K.

The dynamic parameters in Figure 13 contain PC current I, PC contact force F, material hardness H and material resistivity ρ. They can be obtained by simulation models established in the last chapter.

The number of the contact spots n is also a dynamic parameter. On the contact surface of PC, the minimum number of the spots is 3 in theory, and no more than 20 in maximum [34]. The Greenwood-Williamson model [35] is used to accurately determine the number of contact spots n; as shown in Figure 14, if the distance of contact surface and reference plane in the rough surface is d, there will be contact at any summit whose height z is greater than d, and the number of the contact spots n can be expressed as

$$n=N\int_d^{\infty}\varphi(z)\mathrm{d}z \tag{15}$$

where $\varphi(z)$ is the distribution of the height of summits, and N is the number of the summits. The $\varphi(z)$ changes with time due

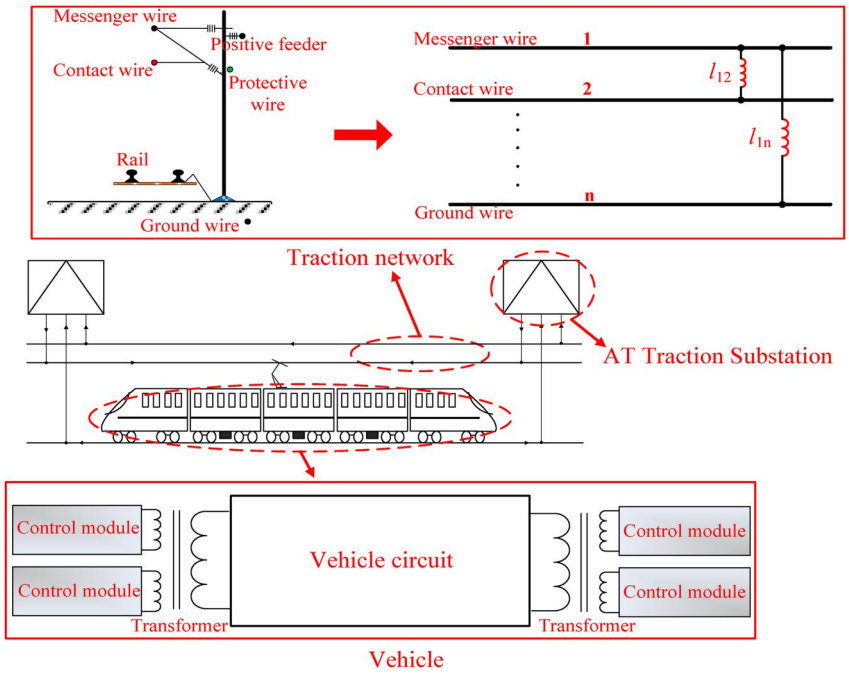

FIGURE 12 Vehicle-grid model

TABLE 2 Simulation parameters of vehicle

Parameters	Value
High voltage cable equivalent resistance	0.014 mΩ/m
High voltage cable equivalent inductance	0.000131093 mH/m
High voltage cable equivalent capacitance	0.00041162 μF/m
Vehicle equivalent resistance	0.225 mΩ/m
Vehicle equivalent inductance	0.001103375 mH/m
Carbon brush resistance	0.05 Ω
Stator resistance	0.15 Ω
Stator self-inductance	0.02682 H
Voltage proportional parameter	0.45
Voltage integral parameter	2.8
Current proportional parameter	0.65

to the relative motion of PC and is difficult to determine accurately. In engineering calculation, the $\varphi(z)$ can be replaced by a normal distribution [24], and combining with the extreme value of contact spots, the number of the contact spots n is N (11.5,1).

The parameter θ_G is the boiling point of contact wire material in Figure 13, and the parameter p represents every node in which spot vaporisation and electric spark happens in the whole calculation process. The electric spark rate η can be expressed as

$$\eta = \frac{p}{k} \tag{16}$$

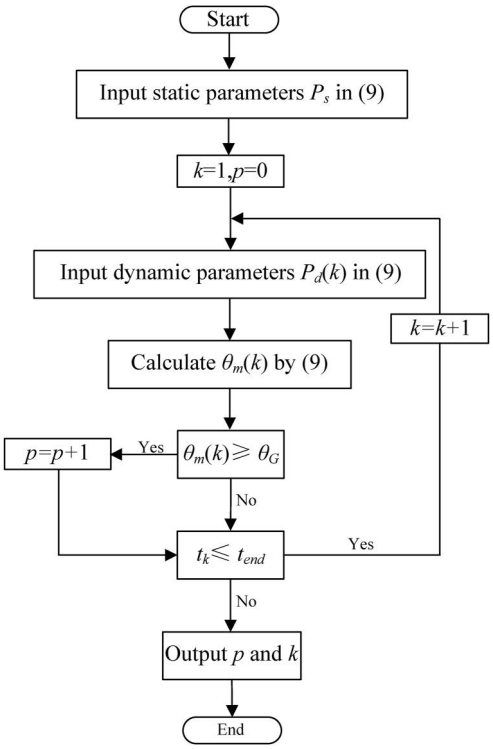

FIGURE 13 Calculation flow of electric spark occurrence

4.1 | Influence of pantograph-catenary interaction on electric spark

From the perspective of PC relationship, the violent interaction of PC, which is mainly caused by irregularity [36],

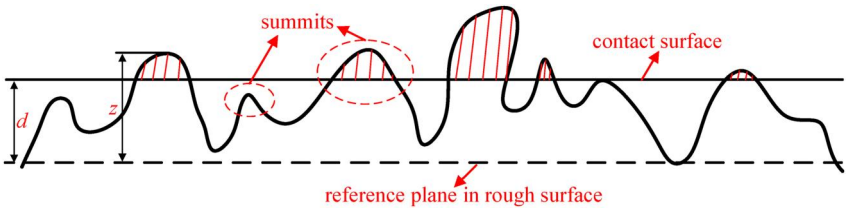

FIGURE 14 Contact of rough surfaces

leads to the electric spark during trains' operation. Under the condition that pantograph and catenary keep contact, the contact force can reflect the irregularity of PC. Based on the PC dynamic structure model, an irregularity parameter is introduced into the simulation in order to obtain different contact forces under the influence of irregularity. Irregularity parameters are expressed as [37],

$$y(k) = \frac{1}{2}A\left[1 - \cos\left(\frac{2\pi x}{\lambda}\right)\right] \tag{17}$$

where A is the amplitude, and λ is the wavelength of irregularity wave.

During the process of simulation, the amplitude A in (16) is used to express varying degrees of irregularity, and the contact force $F(k)$ obtained by simulation is substituted into the flow of Figure 13 as a dynamic parameter for calculation. Calculation results are shown in Figure 15a. The specific calculation parameters are $A_1 = 0.0005$ m, $A_2 = 0.001$ m, $A_3 = 0.0015$ m, $I = 300$A as a static parameter, and $H = 360$ Mpa as a static parameter, respectively. Calculation results are shown in Figure 15b and Table 3.

It can be found in Figure 15a and Table 3 that a higher irregularity tends to cause a higher fluctuation and standard deviation of contact force, which is essentially the decrease of stability of contact force. In the above situation, the contact force is more likely to reach a lower value. Based on (9), the temperature of spots θ_m is more likely to rise to the boiling point of conductor material, and it will cause a higher spark rate in the above situation, as shown in Figure 15b and Table 3.

From the perspective of PC operating environment, the environmental wind is also a main factor affecting PC interaction [38], which leads to the electric spark. The wind-induced vibration of catenary is considered in the PC dynamic structure model in order to analyse the influence of PC interaction under different conditions of environment wind (including wind speed v_w and wind attack angle θ_A). The conditions of environment wind are listed in Table 4.

As the same with the calculation process of irregularity influence on the spark rate, the contact force $F(k)$ under different wind conditions is obtained and substituted into the flow of Figure 13 as a dynamic parameter; other calculation parameters are $A = 0$m, $I = 300$A and $H = 360$Mpa as a static parameter, respectively. Calculation results are shown in Figure 16 and Table 5.

The calculation results in Figure 16 and Table 5 indicate that the increase of wind speed and wind attack angle leads to the increase of standard deviation of contact force and leads to a higher spark rate in the PC system.

4.2 | Influence of pantograph-catenary current on electric spark

From the perspective of train operation state, different train speed or process of acceleration and braking will influence the current between pantograph and catenary, and the spark rate will be influenced according to Equation. (9).

The model in Figure 12 is used to simulate the PC current, and 10 continuous states of train operation (T_1-T_{10}) are considered. The train accelerates from standstill to 119 km/h in T_1 and moves uniformly under the speed of 119 km/h in T_2, then slows down from 119 km/h to 89 km/h in T_3, and then keeps uniform speed under 89 km/h in T_4. Afterwards, the train accelerates from 89 km/h to 178 km/h in T_5 and moves uniformly under the speed of 178 km/h in T_6. After that, the train slows down from 178 km/h to 105 km/h in T_7 and then keeps uniform speed under 105 km/h in T_8, then slows down from 105 km/h to 0 km/h in T_9, and finally keeps standstill in T_{10} (the power supply is not stopped). The simulation results of PC current are shown in Figure 17.

The results of PC currents are substituted into the flow of Figure 13 as the dynamic parameter $I(k)$, and the other parameters are $A = 0.001$ m as a static parameter and $H = 360$Mpa as a static parameter. The calculation results of the spark rate are shown in Figure 18 and Table 4.

Comparing the calculation results in Figure 18a and Figure 18b, it is obvious that the spark rates under acceleration and braking of train operation are much higher than those under uniform speed. In the situation of variable speed of train operation, large acceleration and deceleration will lead to the high spark rate. In the situation of uniform speed of train operation, the spark rate will increase with the train speed.

Table 6 shows the spark rate corresponding to the average current of each continuous state of train operation, and the average spark rate will increase dramatically as average current increases. Combining with the above results, it can be inferred that the change of train running state and speed will lead to the increase of contact current, which will also lead to the increase of spark rate.

4.3 | Influence of contact wire material

From the perspective of material, the engineering test shows that replacing the material of contact wire will improve the spark rate in the PC system [39]. Based on (9), the influence of contact wire material is expressed by hardness H and resistivity ρ of contact wire and pantograph head. The resistivity should have a more dramatic influence on the spark rate, but the

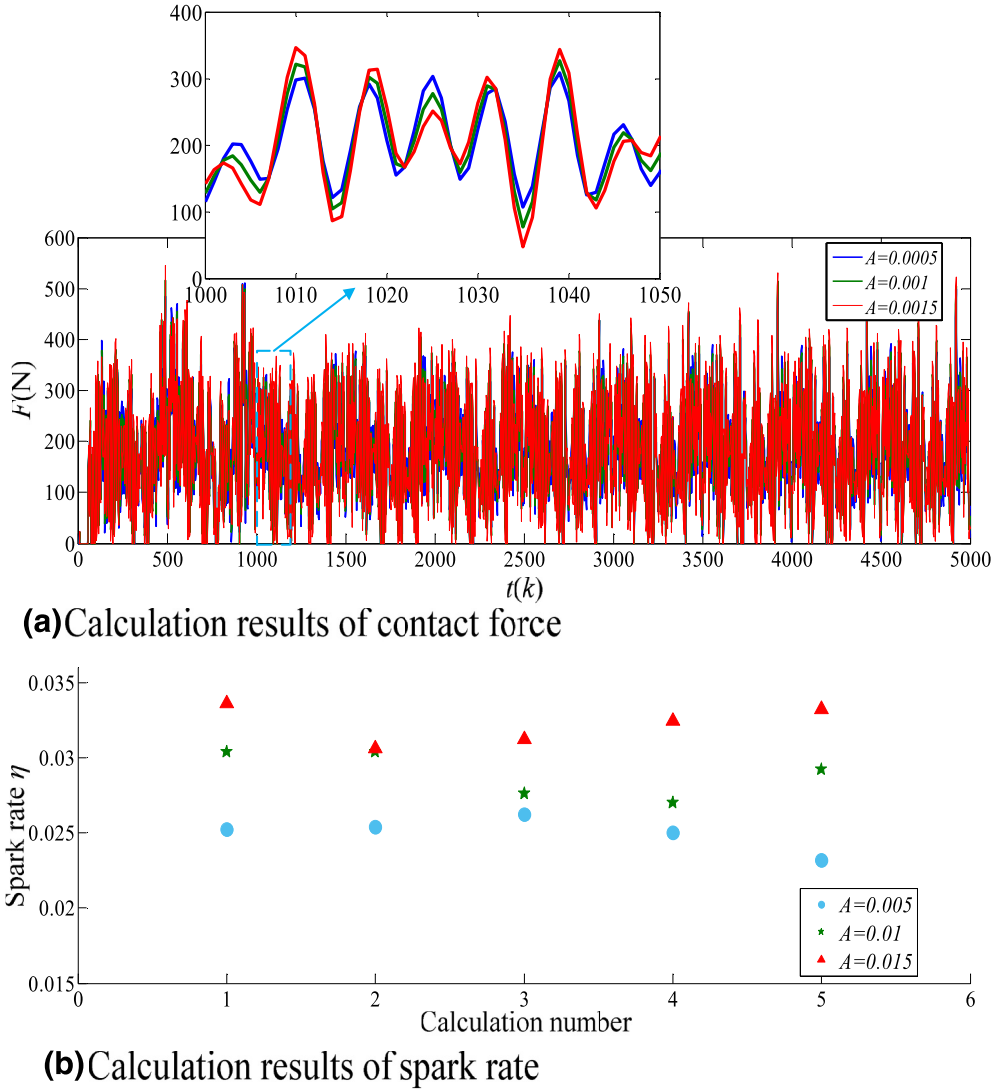

FIGURE 15 Calculation results of electric spark rate under different irregularities

TABLE 3 Calculation results of average spark rate corresponding to contact force

Irregularity A/m	Standard deviation of contact force	Average value of spark rate η
0.0005	92.99	0.0252
0.001	97.79	0.0291
0.0015	105.21	0.0327

TABLE 4 Conditions of environment wind

Condition	Wind speed v_w/m·s^{-1}	Wind attack angle θ_A/°
W_1	20	20
W_2	20	40
W_3	20	60
W_4	30	20
W_5	30	40
W_6	30	60

resistivity of slide plate of pantograph is much bigger than the resistivity of contact wire so that the resistivity can hardly affect the results in this calculation.

The contact wire in the electrified railway system is mainly made by copper alloy at present. Nine kinds of representative contact wire are used to calculate the spark rate, including copper-silver alloy, copper-tin alloy, copper-cadmium alloy, copper-magnesium alloy and copper-zirconium alloy. The hardness of the materials is listed in Table 7 and substituted into the flow of Figure 13. As the dynamic parameters, $A = 0.001$ m and $I = 300$A as the static parameters. Calculation results of the spark rate are shown in Table 7 and Figure 19.

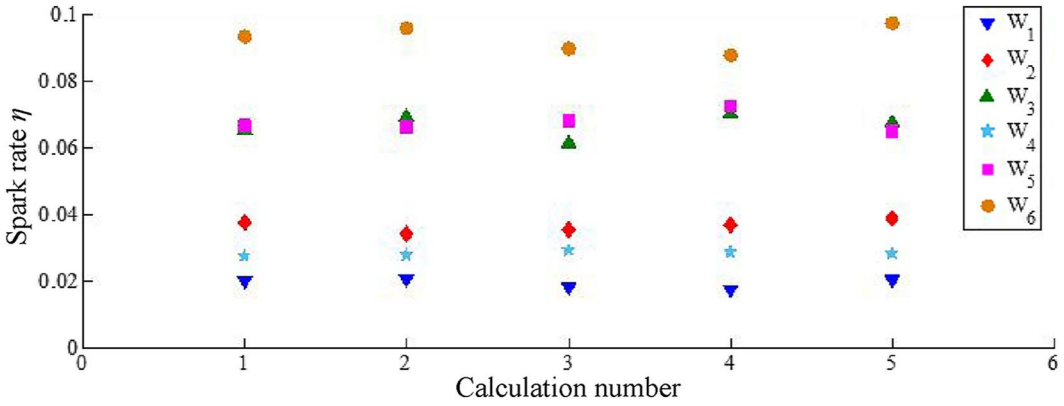

FIGURE 16 Calculation results of the electric spark rate under different environment wind

Condition	Standard deviation of contact force	Average value of spark rate η
W_1	82.32	0.0189
W_2	112.45	0.0371
W_3	158.79	0.0648
W_4	96.16	0.0274
W_5	168.02	0.0708
W_6	204.57	0.0925

TABLE 5 Calculation results of the average spark rate corresponding to contact force

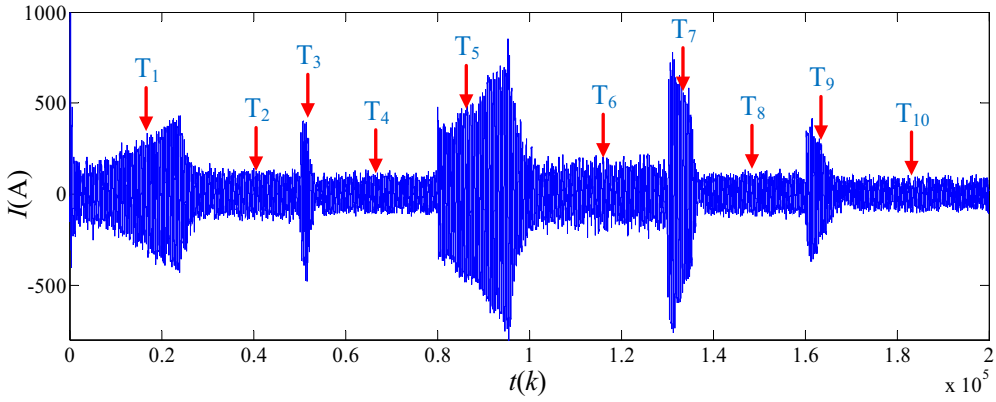

FIGURE 17 Contact current between pantograph and catenary

It can be seen from Figure 19 that the material attribute of contact wire will affect the spark rate, and the two kinds of copper-zirconium alloys have relatively high spark rates while the copper-silver alloys have relatively low spark rates. Based on Equation. (9), the alloy has higher hardness which causes a higher spark rate.

5 | VERIFICATION

The experiment results from Ref. [16] are used to verify the validity of the electric spark discharge model built. In Ref. [16], a scale-down system, which simulates the interaction of PC is established to analyse the electric contact characteristics of PC. The values of contact resistance under different contact force and contact current are measured by the experiment, as shown in Figure 20a.

In order to make the same conditions as the experiment, the material parameters of PC system and the dynamic range of contact current and contact force, which are the same with the experiment, are considered in the verification calculation, as shown in Table 8. Based on the electric spark discharge model in chapter II and the data of contact force and contact current in chapter IV, the values of contact resistance are calculated; the calculation results are shown in Figure 20b.

It can be found in Figure 20 that the contact resistance results calculated by the electric spark discharge model under the same conditions with the experiment matches well with the

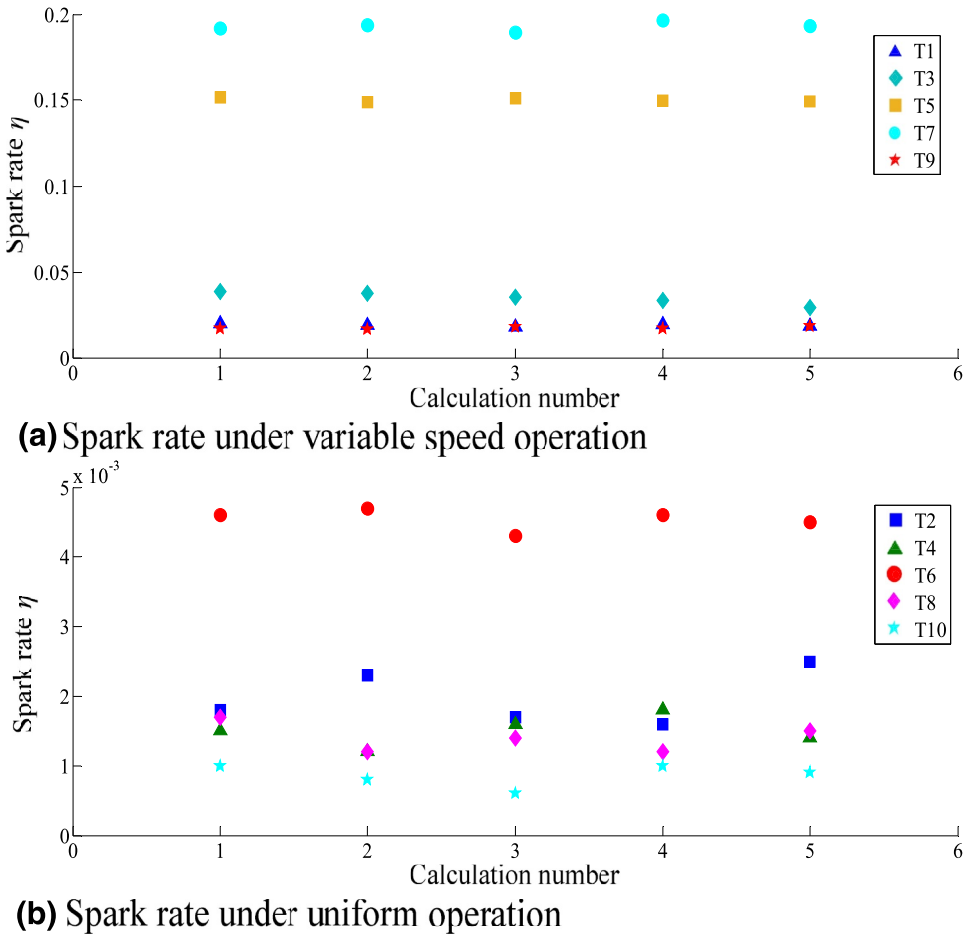

FIGURE 18 Calculation results of the electric spark rate under different current

TABLE 6 Calculation results of the average spark rate corresponding to contact current

Continuous state of train operation	Average value of contact current/A	Average value of spark rate η
T_1	146.75	0.01896
T_2	65.49	0.00198
T_3	161.48	0.03625
T_4	54.78	0.00148
T_5	303.21	0.15005
T_6	92.12	0.00454
T_7	324.09	0.19297
T_8	59.18	0.00152
T_9	139.68	0.01743
T_{10}	42.79	0.00086

results in experiment; the average error is 4.88% and the maximum error is 8.71%. The contact resistance is the key parameter, which reflects the state of electrical contact directly. The comparison result in Figure 20 indicates that the electric spark discharge model established is effective in analysing the PC electrical contact problem.

6 | CONCLUSION

Aiming at the electric spark phenomenon between pantograph and catenary in electrified railways, this paper studies electric spark discharge between PC during train operation. The conclusions are listed as follows:

Contact wire type	Hardness/Mpa	Average value of spark rate η
Cu-0.1Ag (M1)	367	0.0324
Ag-0.07Sn-Cu (M2)	409	0.0384
Cu-Cd (M3)	457	0.0467
Cu-0.7Cd (M4)	413	0.0402
Cu-Mg (M5)	490	0.0502
Cu-0.6 Mg (M6)	500	0.0520
Cu-0.31Cr-0.07Zr-0.02Si (M7)	555	0.0613
Cu-Cr-Zr (M8)	620	0.0719
Cu-0.1Ag-Zr (M9)	580	0.0648

TABLE 7 Calculation results of the average spark rate corresponding to the contact material

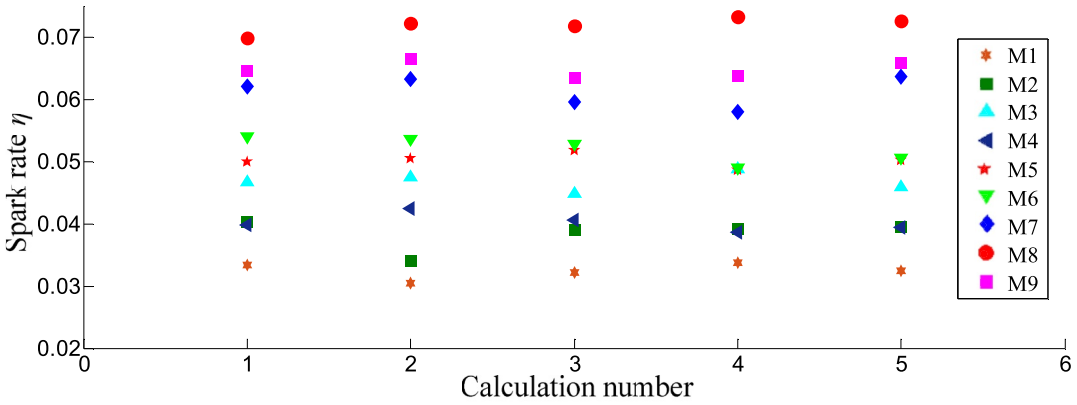

FIGURE 19 Calculation results of the electric spark rate under different materials

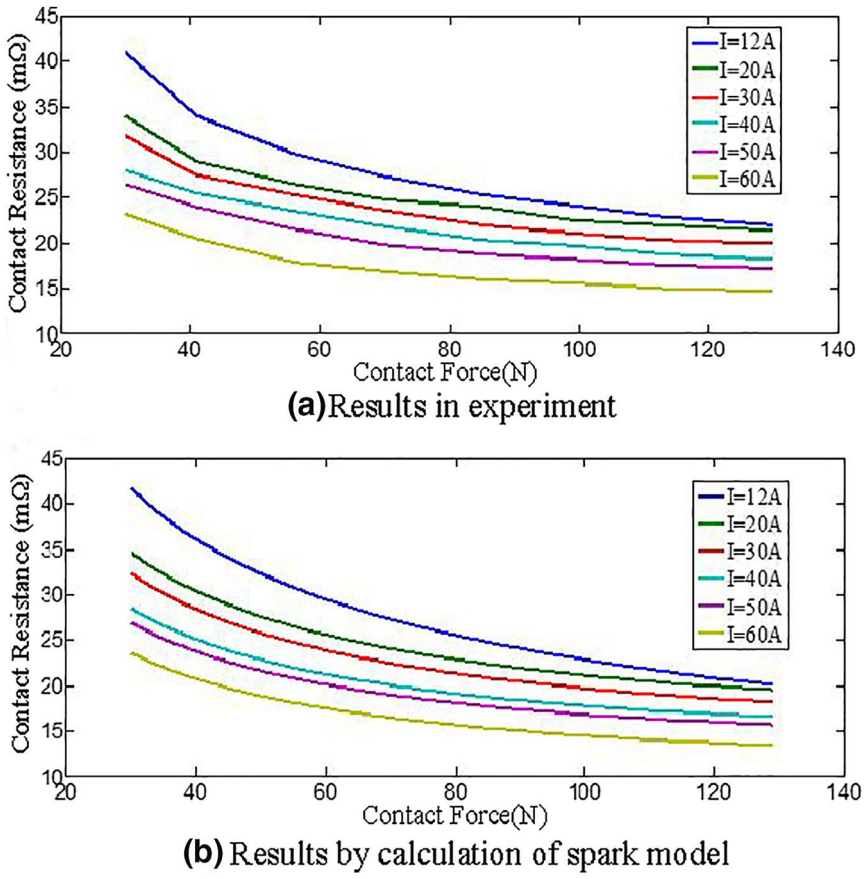

FIGURE 20 Contact resistance results in experiment and by the spark model

TABLE 8 Parameters in verification calculation

Parameter	Value
Resistivity of pantograph ρ_1	7×10^{-6} Ω/m
Resistivity of contact wire ρ_2	2.39×10^{-8} Ω·m^2/m
Hardness of the soft one H	359Mpa
Contact current I	12∼60 A
Contact force F	30N∼130 N

(1) The mechanism of electric spark discharge is analysed combined with the classical electrical contact theory and practical factors of the PC system. It shows that the vaporisation of contact spots causes the interruption of PC contact, and forms the electric spark discharge under the action of voltage difference in the PC system. The electric spark discharge model is proposed combining with the spark discharge mechanism and spot temperature rise formula, which can be used to determine the occurrence of spark discharge of PC and calculate the spark rate.
(2) Through the calculations of the electric spark discharge model, the results show the factors, including contact force, contact current and contact material, which corresponding to different operation status and configuration of train, have different influence degrees on spark discharge.

This study not only reveals the mechanism of electric spark and its influence factors but also provides theoretical supports on assessment of PC electrical contact quality and guidance of operation and design on the vehicle-grid system.

7 | DISCUSSION

Electric spark phenomenon occurs frequently in the PC system, which directly affects the PC current collection quality. This paper makes a mechanism analysis and modelling of PC electric spark, which is not involved in the previous research studies of PC current collection quality, and calculates the PC spark rate combining with practical factors of PC, which are not considered in the previous research studies of spark discharge. This paper makes some simplifications in the process of theoretical derivation; a more accurate spark model would be obtained if detailed conditions are considered such as various spot shapes and distributions. Moreover, there may be other factors which affect the occurrence of spark such as PC operation environment and PC interaction, and more results about PC electric spark may be found if they are taken into consideration.

ACKNOWLEDGEMENT

This work was supported in part by the National Nature Science Foundation of China (U1734202), Science and Technology Innovation Talents of Sichuan Science and Technology Plan (2021JDRC0008) and Research Project of China Railway Eryuan Engineering Group Co. Ltd (KYY2020033(20-21)).

CONFLICT OF INTEREST

None.

DATA AVAILABILITY STATEMENT

All data, models, and code generated or used during the study appear in the submitted article.

ORCID

Hongyi Zhou https://orcid.org/0000-0001-8890-4941
Fuchuan Duan https://orcid.org/0000-0003-1047-3736
Zhigang Liu https://orcid.org/0000-0003-4154-5587
Yang Song https://orcid.org/0000-0002-7699-5855

REFERENCES

1. Song, Y., et al.: A spatial coupling model to study dynamic performance of pantograph-catenary with vehicle-track excitation. Mech. Syst. Signal Process. 151, 107336 (2021)
2. Song, Y., Liu, Z., Lu, X.: Dynamic performance of high-speed railway overhead contact line interacting with pantograph considering local dropper defect. IEEE Trans. Veh. Technol. 69(6), 5958–5967 (2020)
3. Chen, J., et al.: Automatic defect detection of fasteners on the catenary support device using deep convolutional neural network. IEEE Trans. Instrum. Meas. 67(2), 257–269 (2018)
4. Shabana, A., Zaazaa, K., Sugiyama, H.: Railroad vehicle dynamics: a computational approach. CRC Press (2007)
5. Collina, A., Bruni, S., Bruni, S.: Numerical simulation of pantograph-overhead equipment interaction. Veh. Syst. Dyn. 38(4), 261–291 (2002)
6. Pappalardo, C., et al.: Contact force control in multibody pantograph-catenary systems. Multi-body Dynamics. 230(4), 307–328 (2016)
7. Seo, J., Sugiyama, H., Shabana, A.: Three-dimensional large deformation analysis of the multibody pantograph/catenary systems. Nonlinear Dynam. 42(2), 199–215 (2005)
8. Holm, R.: Electrical contact hand book. Springer-verlag (1958)
9. Williamson, J.: The microworld of the contact spot. Proceedings of IEEE Holm Conference on Electrical contacts, 27, 1–10 (1998)
10. Malucci, R.: Multispot model of contacts based on surface features, pp. 625–634. IEEE International Conference on Electrical contacts (1990)
11. Yasuhiro, F., Norihiko, S.: The effect of the distribution of a-spots in the peripheral part of an apparent contact point on constriction resistance, pp. 302–305. IEEE Holm Conference on Electrical Contacts (2017)
12. Timsit, R.: Electrical conduction through small contact spots. IEEE Trans. Compon. Packag. Technol. 29(4), 727–734 (2006)
13. Li, L., Li, C., Feng, Y.: Analysis of electrical contact temperature rise in spark gap switches with graphite electrodes. IEEE Trans. Dielectr. Electr. Insul. 18(4), 1307–1313 (2011)
14. Zhang, Y., Zhang, Y., Song, C.: Arc discharges of a pure carbon strip affected by dynamic contact force during current-carrying sliding. Materials. 11(5), 796–811 (2018)
15. Chen, Z., Shi, Y., Shi, G.: Calculation model of the contact resistance between pantograph slide and contact wire. Trans. China Electrotech. Soc. 28(5), 188–195 (2013)
16. Wang, W., Dong, A., Wu, G.: Study on characterization of electrical contact between pantograph and catenary, pp. 1–6. IEEE Holm Conference on Electrical Contacts (2011)
17. Barmada, S., et al.: Arc detection in pantograph-catenary systems by the use of support vector machines-based classification. IET Electr. Syst. Transp. 4(2), 45–52 (2014)
18. Karaduman, G., Karakose, M., Akin, E.: Deep learning based arc detection in pantograph-catenary systems' International Conference on Electrical and Electronics Engineering, pp. 904–908. (2017)
19. Aydin, I., Yaman, O., karakose, M.: Particle swarm based arc detection on time series in pantograph-catenary system. IEEE International Symposium on Innovations in Intelligent Systems and Applications Proceedings, 344–349 (2014)

20. Yaman, O., Karakose, M., Aydin, I.: Image processing and model based arc detection in pantograph catenary systems, Signal Processing and Communications Applications Conference, pp. 1934–1937. (2014)
21. Kojima, H., et al.: Dependence of spark conditioning on breakdown charge and electrode material under a non-uniform electric field in vacuum. IEEE Trans. Dielectr. Electr. Insul. 23(5), 3224–3230 (2016)
22. Rose, J., et al.: Nonlinear spark resistance and capacitive circuit models of electrostatic discharge. IEEE Trans. Plasma Sci. 48(2), 462–470 (2020)
23. Vanny, R., Ohyama, R.: Time lag characteristics of spark discharge in humid air with increased voltage. IEEE Trans. Dielectr. Electr. Insul. 25(4), 1487–1491 (2018)
24. Braunovic, M., Knchits, V., Myshkin, N.: Electrical contacts fundamentals, applications and technology. CRC Press (2007)
25. Thomas, T.: Rough surfaces. Longman (1982)
26. Chen, L.: Contact resistance model and its application. High Volt. Appar. 29(2), 34–40 (1993)
27. Turner, M., Swinnerton, B.: Sparking and arcing in electrical machines. Proc. Inst. Electr. Eng. 113(8), 1376–1386 (1966)
28. Song, Y., et al.: Nonlinear modelling of high-speed catenary based on analytical expressions of cable and truss elements. Veh. Syst. Dyn. 53(10), 1455–1479 (2015)
29. Song, Y., et al.: Active control of contact force for high-speed railway pantograph-catenary based on multi-body pantograph model. Mech. Mach. Theor. 115, 35–59 (2017)
30. Lu, X., et al.: Estimator-based multiobjective robust control strategy for an active pantograph in high-speed railways. Proc. Inst. Mech. Eng. - Part F J. Rail Rapid Transit. 232(4), 1064–1077 (2017)
31. Song, Y., Rannquist, A., Navik, P.: Assessment of the high-frequency response in the Railway Pantograph-Catenary interaction based on numerical simulation, IEEE Trans. Veh. Technol. El69(10), 10596–10605, (2020)
32. Huang, K., et al.: Evaluation scheme for EMI of train body voltage fluctuation on the BCU speed sensor measurement. IEEE Trans. Instrum. Meas. 66(5), 1046–1057 (2017)
33. Cheng, Y., Liu, Z., Huang, K.: Transient analysis of electric arc burning at insulated rail joints in high-speed railway stations based on state-space modeling. IEEE Transactions on Transportation Electrification. 3(3), 750–761 (2017)
34. Shobert, E.: Carbon brushes. Chemical Publ (1965)
35. Greenwood, J., Williamson, J.: Contact of nominally flat surfaces. Proc. Roy. Soc. A295, 300 (1966)
36. Song, Y., Liu, Z., Anders, R.: Contact wire irregularity stochastics and effect on high-speed railway pantograph-catenary interactions. IEEE Trans. Instrum. Meas. 69(10), 8196–8206 (2020)
37. Wang, H., Liu, Z., Song, Y.: Time-frequency analysis of pantograph-catenary contact force and contact wire irregularity in high-speed railway based on ZAMD. J. China Railw. Soc. 38(1), 41–47 (2016)
38. Song, Y., Zhang, M.: Wind deflection analysis of railway catenary under corsswind based on nonlinear finite element model and wind tunnel test. Mech. Mach. Theor. 168, 1–22, 104608 (2022)
39. Han, T.: Reason analysis for continuous spark in current collection of catenary-pantograph system. Railway Locomotive and Car. 2(3), 58–61 (2003)

How to cite this article: Zhou, H., et al.: Study on electric spark discharge between pantograph and catenary in electrified railway. IET Electr. Syst. Transp. 12(2), 128–142 (2022). https://doi.org/10.1049/els2.12043